

An Impedance Study of the Density of States Distribution in Blends of PM6:Y6 in Relation to Barrierless Dissociation of CT States

Daniel Kroh, Stavros Athanasopoulos, Vojtech Nádaždy, Frank-Julian Kahle, Heinz Bäessler, and Anna Köhler*

In an endeavor to understand why the dissociation of charge-transfer (CT) states in a PM6:Y6 solar-cell is not a thermally activated process, measurements of energy-resolved impedance as well as of intrinsic photoconduction are employed. This study determines the density of states distributions of the pertinent HOMO and LUMO states and obtains a Coulomb binding energy ($E_{b,CT}$) of ≈ 150 meV. This is 250 meV lower than the value expected for a pair of localized charges with 1 nm separation. The reason is that the hole is delocalized in the polymer and the electron is shared among Y6 molecules forming a J-like aggregate. There are two key reasons why this binding energy of the CT state is not reflected in the temperature dependence of the photocurrent of PM6:Y6-diode: i) The e–h dissociation in a disordered system is a multi-step process whose activation energy is principally different from the binding energy of the CT state and can be substantially less than $E_{b,CT}$, and ii) since dissociation of the CT state competes with its intrinsic decay, the dissociation yield saturates once the rate of dissociation grossly exceeds the rate of intrinsic decay. This study argues that these conditions are met in a PM6:Y6-solar cell.

1. Introduction

Blending the polymeric donor material PM6 with the monomeric acceptor Y6 is the basis for an unusually efficient solar cell, yet it is open to discussion why this cell is so efficient.^[1–6] One reason is that the optical gap is as low as 1.45 eV and both components have high oscillator strengths. Therefore, more light is absorbed in a PM6:Y6 solar cell than in a cell with PCBM as an acceptor. It is less obvious, though, why almost no thermal energy is needed to dissociate to optically generated charge transfer states (CT).^[7] The CT state ought to be Coulomb bound but obviously, it is bound only very weakly. One reason is related to the polymeric nature of the donor that favors delocalization of the hole and, concomitantly, reduces the binding energy of the CT state.^[7–10] The morphology of the blend and static disorder also contributes


favorably to CT dissociation.^[9] Recently, it has been suggested that the quadrupole of the Y6 molecule increases the dissociation yield because it gives rise to a repulsive term of the potential energy of a charged donor–acceptor pair.^[7,11] To verify these conjectures requires detailed knowledge of the energetic landscape of a PM6:Y6 blend, which is difficult to determine experimentally. While conventional photoemission is a suitable method to determine the HOMO level, inverse photoemission is experimentally demanding and in principle unsuitable for exploring the LUMO-structure of a two-component system. In order to overcome the latter problem, Neusser et al.^[12] conducted a spectro-electrochemical study to determine the HOMO and LUMO levels in the neat films of PM6 and Y6 as well as their blends with particular emphasis on the film-morphology. While this technique can locate the level-positions, it is inadequate to map the pertinent density of states distributions. For this reason, we resort to energy resolved electrochemical impedance spectroscopy (ER-EIS) to determine the density of the states (DOS) distribution of PM6 and Y6 films and the PM6:Y6 blend.^[13–15] The blend we use was prepared as described by Perdigon-Toro et al.,^[16] and also used in our previous study, where we investigated the role of order on the open-circuit voltage in solar cells.^[1] In particular, we used the same batch of PM6 as in Refs. [16] and [1], and dissolved it with Y6 (from the same supplier, 1-Material Inc.) in CHCl₃ to a total

D. Kroh, S. Athanasopoulos, F.-J. Kahle, A. Köhler
Soft Matter Optoelectronic
Department of Physics
University of Bayreuth
Universitätsstr. 30, 95448 Bayreuth, Germany
E-mail: anna.koehler@uni-bayreuth.de

S. Athanasopoulos
Departamento de Física
Universidad Carlos III de Madrid
Avenida Universidad 30, Leganés, Madrid 28911, Spain

V. Nádaždy
Institute of Physics and Centre for Advanced Material Application
Slovak Academy of Sciences
Dubravska cesta 9, Bratislava 845 11, Slovakia

H. Bäessler, A. Köhler
Bayreuth Institute of Macromolecular Research (BIMF)
University of Bayreuth
Universitätsstr. 30, 95448 Bayreuth, Germany

 The ORCID identification number(s) for the author(s) of this article can be found under <https://doi.org/10.1002/adfm.202302520>

© 2023 The Authors. Advanced Functional Materials published by Wiley-VCH GmbH. This is an open access article under the terms of the Creative Commons Attribution License, which permits use, distribution and reproduction in any medium, provided the original work is properly cited.

DOI: 10.1002/adfm.202302520

concentration of 16 mg mL⁻¹ with a 1.0–1.2 weight ratio and 0.5% CN (v/v, CN/ CHCl₃) as additive. Complementary, we also measure the action spectrum of intrinsic photoconduction in order to determine the electrical gap of neat PM6 and Y6 films.

It turns out that the ER-EIS spectrum of a PM6:Y6 blend is basically a superposition of HOMO and LUMO features of the parent components indicating that blending does not give rise to additional states. It yields a binding energy of the CT state of ≈150 meV. This value is consistent with earlier studies,^[16,17] yet unusually low as compared with an expected Coulomb energy of ≈400 meV. In recent studies,^[1,18] we used an analysis of absorption and PL-spectra in combination with grazing incidence wide angle x-ray scattering (GIWAXS) measurements to associate the presence of J-like aggregates with the high solar cell quantum yields reported by Perdigon-Toro et al.^[16] In the study presented here, we shall now argue further that the low binding energy of the CT state is a consequence of the formation of these J-type aggregates. It implies that the electron in the acceptor-phase is delocalized among two molecules. This lowers the Coulomb energy of the CT state beyond the contribution of hole delocalization in the PM6 polymer.

An important aspect of the current study is the question whether or not the spectroscopically determined binding energy of a CT state ($E_{b,CT}$) is identical to the activation energy of the photocurrent in a PM6:Y6-blend. Supported by kinetic argument and simulations using an analytical hopping model we shall argue that both energies are principally different. While $E_{b,CT}$ is a spectroscopically defined quantity, the thermal activation energy is not, because CT dissociation is a multi-step rate process that depends on the topology and dimensionality of the system, and therefore the activation energy is lower than the binding energy of the CT-state. After all, we shall stress that the yield of CT-dissociation is determined by the trade-off between the rate of escape process and the rate of its intrinsic decay to the ground state. If CT dissociation is fast compared to intrinsic decay, its yield is unity regardless of how much energy an individual jump of a charge carrier in the course of dissociation may cost. This is an important, yet often overlooked argument in the discussion on the activation energy of CT-dissociation.

2. Results

2.1. Photoconduction

Before embarking into ER-EIS experiments, we shall first report on experiments of photoconduction on neat films of only one material. They rest upon the autoionization concept of a molecular solid. Upon generating singlet excitons in a biased neat molecular solid one usually observes a photocurrent. It is mainly of extrinsic nature because singlet excitons do not have enough energy to dissociate and originates from exciton dissociation at an electrode or an impurity^[19] or by bimolecular annihilation of excitons. However, above a threshold energy a higher excited vibronic state can overcome the Coulombic binding energy of a singlet exciton and can autoionize. This gives rise to a superimposed intrinsic photocurrent. The threshold energy for this process defines the electrical bandgap E_g , i.e., the separation between the valence and the conduction states of the system, as compared to the optical gap. The difference between the electrical and the op-

tical gap is the binding energy of the singlet exciton. Pope et al.^[20] and Braun et al.^[21] were pioneers in this research. In the course of our endeavor to characterize the optical properties of conjugated polymers, we drew upon those classic ideas and measured the action spectrum of the photocurrent of the ladder-type poly-paraphenylene (MeLPPP) in order to discriminate between intrinsic and extrinsic photoconduction.^[22] It turned out that there is a threshold energy of 3.8 +/- 0.1 eV above back to which the photocurrent increases sharply. More recently, we measured the impedance spectra of the material and we found that the HOMO–LUMO gap, E_g ; is 3.72 eV Bässler et al.^[15] This agreement proves that both methods to determine E_g are internally consistent.

Single layer devices for external quantum efficiency (EQE) measurements using Y6 and PM6 were fabricated on structured ITO-coated glass substrates. As a hole transport layer, a 15 nm thick layer of MoO₃ on top of the ITO was used. The Y6 layer was spun from chloroform solution (10 mg mL⁻¹), the PM6 layer from chlorobenzene solution (10 mg mL⁻¹), both with a thickness of 100 nm. Last, a 100 nm thick aluminum cathode was evaporated. EQE measurements were performed using a Keithley 236 source-measure-unit under monochromatic illumination from a 450 W tungsten lamp (Osram). All EQE spectra were recorded under short-circuit conditions. For the measurement, the sample was kept in a sample holder under vacuum at room temperature.

We calculated the internal quantum efficiency (IQE) using the absorption profiles we obtained via the transfer matrix algorithm. These calculations were performed using the code provided free of charge by McGehee and coworkers.^[23] The values for the real (n) and imaginary part (k) of the refractive index for glass, ITO and Al were taken from the library provided by McGehee. For MoO₃ we used the values from the free online library RefractiveIndex.INFO.^[24] For PM6 and Y6, we followed the approach presented by McGehee and coworkers. Thus, we used the refractive index $n(\lambda)$ for Y6 and PM6, determined by Kerremans and coworkers^[25] and only measured the absorption coefficient of the respective materials from which we then calculated the k -values according to $k = \lambda \alpha / 4\pi$, where λ is the wavelength of the incident light and α is the absorption-coefficient.^[23]

In **Figure 1** we show the absorption spectra as well as the IQE spectra of PM6 (Figure 1a) and Y6 (Figure 1b). The onset of the IQE spectra coincides with the absorption threshold. With increasing photon energy, the IQE spectra saturate (IQE_{sat}) yet above a certain threshold the photocurrent increases again. We associate this increase of the intrinsic photocurrent with autoionization of higher excited states. At even higher energies, e.g., at 3.2 eV for PM6 and 2.6 eV for Y6, we notice a reduced increase or even decrease. Evidently, there are other decay channels for the singlet exciton opening up that compete with autoionization, such as conceivably pathways related to singlet fission or other processes. To determine the electrical gap E_g we plot the $(IQE(h\nu) - IQE_{sat})^{1/2}$ versus $h\nu$ (Figure 1c,d). This is an empirical way to quantify the increase of the number of intrinsically generated charge carriers as a function of the excess photon energy because the number of charges that escape from their Coulomb funnel increases approximately quadratically with their excess energy.^[26] This procedure yields the HOMO–LUMO gaps, i.e., the electrical gaps, $E_g(\text{PM6}) = 2.51$ eV (± 0.10 eV) and $E_g(\text{Y6}) = 1.77$ eV (± 0.10 eV)

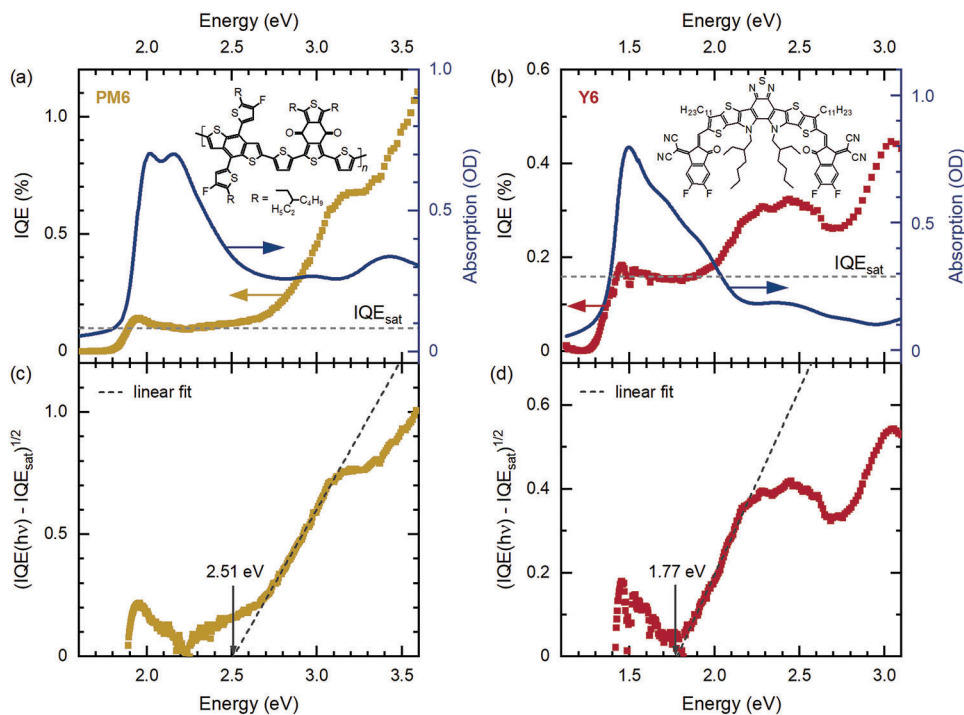


Figure 1. Internal quantum efficiency (*IQE*) spectra for a) PM6-only and b) Y6-only device under short-circuit conditions with its absorption on the right axis and the material structure on the top. Plot of the square root of $IQE(h\nu) - IQE_{sat}$ versus $h\nu$ with a linear fit to determine the electrical gap E_g for c) PM6-only and d) Y6-only devices.

2.2. Impedance Spectroscopy (ER-EIS)

ER-EIS is a spectroscopic technique to map the density of states (DOS) distribution of an organic solid in contact with an electrolyte via a redox-reaction. It is an elaborate version of conventional cyclic voltammetry used to determine ionization potentials and electron affinities of organic materials in solution. In brief, an organic film is deposited onto a conductive substrate, e.g., an ITO covered glass or doped Si, and immersed into an electrolyte with an Ag/AgCl reference and a Pt auxiliary wire electrode. Between film and the electrolyte, a Helmholtz layer is established. Experimentally, one measures the charge transfer resistance at the interface between the electrolyte and the organic semiconductor by superimposing a periodic perturbation of the applied potential. Reversible charge transfer from ions of the electrolyte to the semiconductor will occur once the applied voltage compensates the difference between those states and gives rise to the real component of the measured impedance. Since the interfacial resistance depends on the number of the available states at the semiconductors surface, a scan of the resistance as a function of the applied voltage will translate into the distribution of HOMO and LUMO states of the semiconductor. For more information on the ER-EIS technique see Refs. [13–15].

In the present experiments, thin films, typically 100 nm thick, were deposited onto a tin-oxide (ITO) covered glass plate. Y6 films were spin-coated from chloroform solution (16 mg mL^{-1}), PM6 from chlorobenzene solution (10 mg mL^{-1}), and PM6:Y6-blends (1:1.2 ratio) from chloroform solution (16 mg mL^{-1}).

Figure 2a shows the ER-EIS spectrum of a PM6 film, i.e., the density of states distributions (DOS) of HOMO and LUMO

states. The tails of both DOSs are perfect Gaussians distributions with standard deviations $\sigma_H = 100 \text{ meV}$ and $\sigma_L = 43 \text{ meV}$, respectively. The maxima of the HOMO and LUMO distributions are at -5.82 and -3.32 eV , respectively. It implies an electrical gap E_g (PM6) of 2.50 eV . This is in agreement with the threshold for intrinsic photoconduction ($2.51 \pm 0.10 \text{ eV}$) but is by 0.25 eV higher than the value inferred from spectral voltammetry (2.25 eV).^[12] The most likely reason for this discrepancy is that in the latter technique the level position is inferred from the onset of the feature in the voltammetry-spectrum. A broad HOMO distribution—as measured for a neat PM6 film ($\sigma = 100 \text{ meV}$) can therefore translate into an erroneously lower HOMO level and, thus, to a lower value of E_g .

Interpreting the ER-EIS spectrum of an Y6 film is less straightforward because Y6 tends to crystallize^[1,18,27–31] and the morphology of the film depends somewhat on the choice of the solvent and processing conditions.^[29,32–37] GIWAXS measurements have shown that our Y6 films exhibit long-range order that is distinctly different from the ordered regions characterized by π - π stacking between chains that prevail in PM6.^[1,18] The spectrum shown in Figure 2a indicates that from -6.2 to -5.0 eV the HOMO-DOS decays smoothly except for a superimposed local maximum at -5.99 eV . The LUMO feature is a spike at -4.34 eV , accompanied by a weak shoulder at lower energies. Beyond -4.34 eV there is a broad local maximum followed by another local maximum at -3.0 eV . It is straightforward to assume that the LUMO spectrum is related to the film morphology. Temperature-dependent absorption spectra on Y6 in solution and on Y6 films show that Y6 forms aggregates with predominate J-like character embedded in an amorphous phase.^[18] It is straightforward to associate

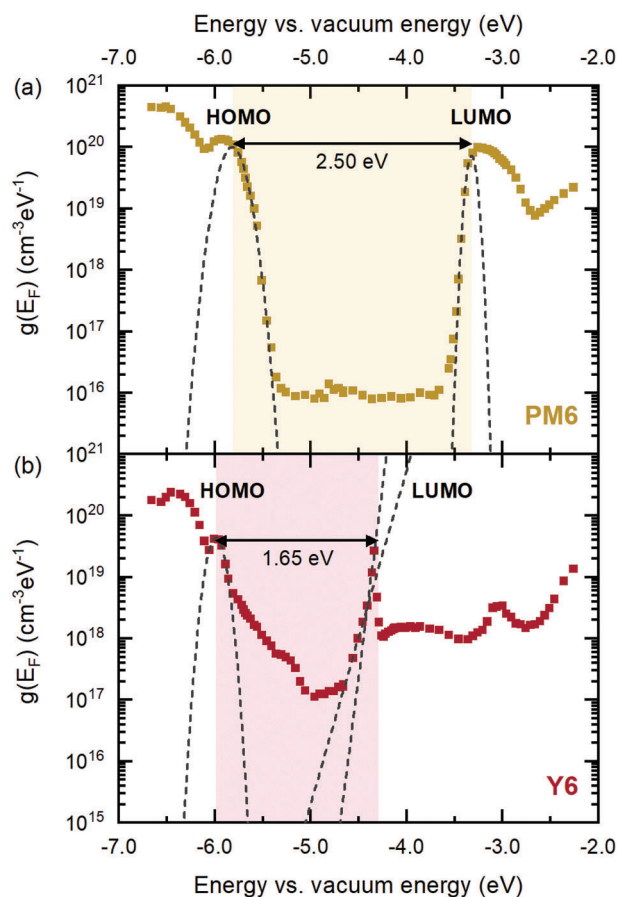


Figure 2. The DOS function $g(E_F)$ for HOMO and LUMO states of a) PM6 and b) Y6 film inferred from ER-EIS measurements. The dashed lines indicate Gaussian and exponential fits. The arrows indicate the energetic HOMO–LUMO gap.

the spike of the LUMO feature in an Y6 film to LUMO states of well-ordered crystallites and the broad feature beyond -4.20 eV to the amorphous phase. The weak tail associated with central spike we associate with states at the grain boundaries of the crystallites. Alam et al.^[38] noticed a similar spike at -4.3 eV in ER-EIS spectra of donor–acceptor blends with ITIC, an acceptor that is chemically similar to Y6. They associated it with a Fano resonance between a local and a continuum of states. We conjecture that the spike is a characteristic signature of well-ordered aggregates. The following results of PM6:Y6 blends will support this reasoning. Taking the HOMO feature at -5.99 eV and the LUMO-spike at -4.34 eV we end up with an electrical gap E_g of 1.65 eV for Y6. This is in excellent agreement with the value of 1.64 eV inferred from spectral voltammetry^[12] and in fair agreement with the threshold energy for intrinsic photoconduction (1.77 eV \pm 0.10 eV).

The key experimental result of this study is the ER-EIS spectrum of the PM6:Y6 blend, shown in the bottom of **Figure 3**. To illustrate more clearly the changes that occur upon blending we include in **Figure 3a** also the spectra of the single materials. The spectrum of the blend is basically the sum of the spectrum of the components albeit with characteristic modifications: i) In the blend the unusually high density of states within the forbidden

zone of the Y6 spectrum has vanished. This suggests that the states within the forbidden zone are in some way related to grain boundaries between the crystallites in the neat Y6 film that are eliminated upon blending with PM6. ii) The HOMO spectrum of the blend is entirely dominated by that of the donor PM6 and the Gaussian width is diminished from 100 meV of the neat film to 74 meV in excellent agreement with literature.^[11] iii) In the blend, the LUMO spectrum of Y6 is shifted by ≈ 100 meV. Such an effect was already noticed in the course of our earlier study on MeLPPP:PCBM cells and can be attributed to different dielectric screening on the blend with respect to neat films or to interfacial dipoles.^[39] iv) Both the spike and the associated tail below 4 eV are weakly broadened. Obviously, blending decreases the structural order within the crystalline domains and at the grain boundaries and the LUMO features acquire Gaussian shapes with standard deviations of 60 meV (crystallites) and 100 meV (tail states). This disorder-controlled line-broadening indicates that the sharp LUMO feature should not be assigned to a Fano resonance.^[38] v) The electrical gap between the centers of the HOMO features of PM6 and the boundary and central crystallite LUMO features of Y6 are 1.44 and 1.59 eV, respectively. vi) The LUMO feature on the PM6 spectrum and the second LUMO feature of Y6 are amalgamated.

3. Discussion

Interpreting the binding energies of singlet excitons in neat PM6 and Y6 films appears to be straightforward. The difference between the electrical gap of 2.50 eV of a PM6 film and the 0 – 0 -transition of S_1 – S_0 transition at 1.90 eV yields an electrical gap of 0.60 eV. Identifying it with the Coulomb energy of a pair of point-like charges in a dielectric medium with a dielectric constant of 3.5 translates into an on-chain e–h pair with a separation of 0.7 nm. For a Y6 film we find that the electrical gap is 1.65 eV and the origin of the S_1 – S_0 transition is 1.40 eV. This yields a binding energy of a pair of point-like charges of 0.25 eV and translates into an unusually large e–h separation of 1.6 nm. The likely reason is that since Y6 molecules form J-like aggregates the charges can delocalize among the pair partners (vide infra).

The observation that the ER-EIS spectrum of a PM6:Y6 blend is basically a superposition of the HOMO and LUMO DOS distributions of the components with only marginal shift (<100 meV) proves that blending does neither create new states nor modifies their energetic positions appreciably. Obviously, the quadrupole moment of the Y6 molecule does not alter the HOMO or LUMO levels noticeably when a donor–acceptor pair is formed.

Upon optical excitation of a PM6:Y6 blend singlet excitons are created either in Y6 domains or via energy transfer from PM6 to Y6. Some excitons are lost by fluorescence from Y6 domains, but their majority migrates to the domain boundaries at which holes are transferred to a PM6 chains thereby generating CT states. Their energy is difficult to measure because the CT emission is weak and overlaps with the residual fluorescence of Y6. By subtracting the photoluminescence from the electroluminescence of a PM6:Y6 diode, Perdigon-Toro et al.^[16] came up with a CT emission spectrum with a peak at 1.15 eV with origin at 1.30 eV. When we subtract the value of the CT origin from our value of 1.44 eV for the difference between the centers of the HOMO and LUMO

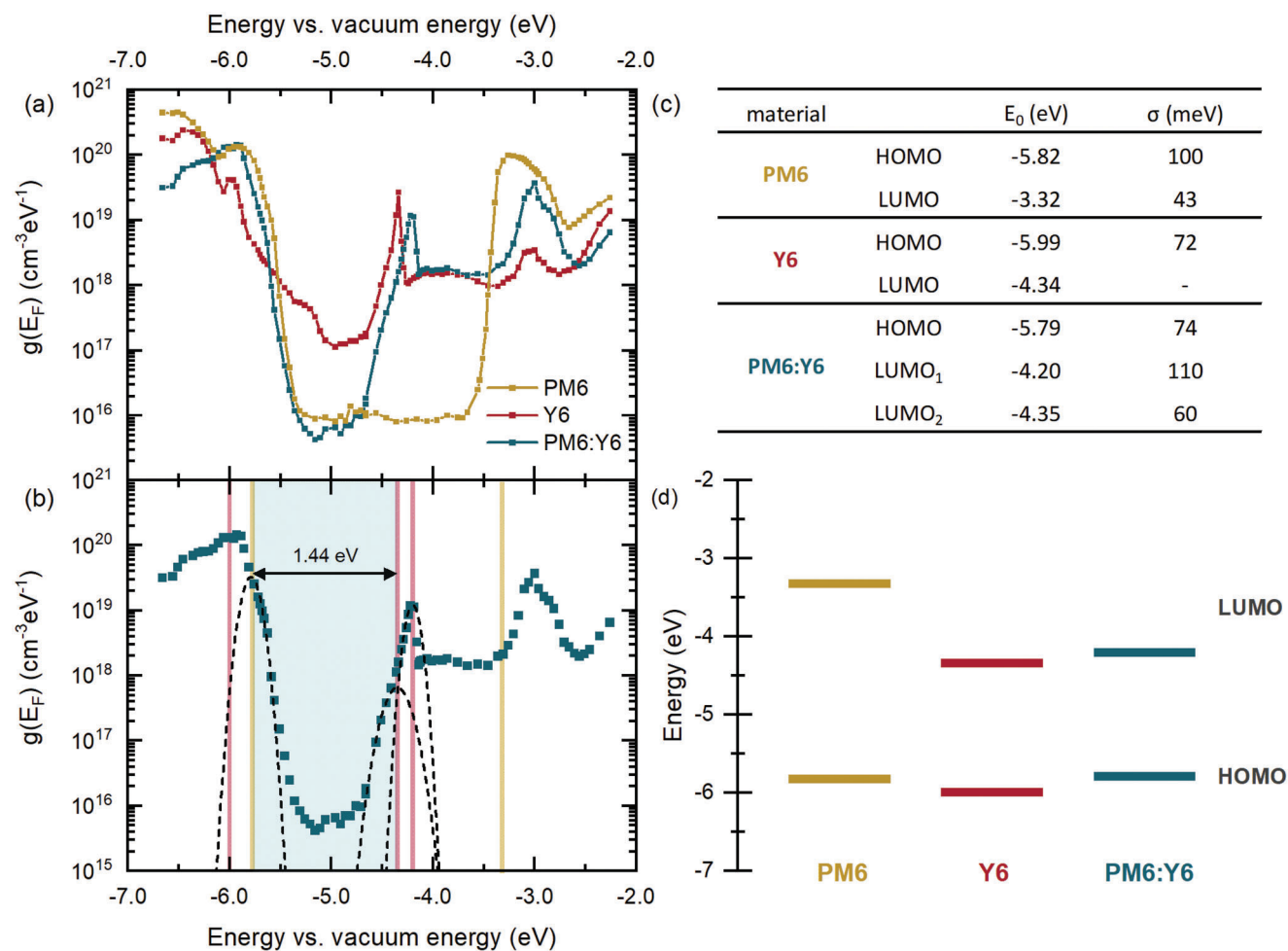


Figure 3. a) The DOS function $g(E_F)$ for HOMO and LUMO states of a PM6, Y6 and PM6:Y6 film inferred from ER-EIS measurements. b) $g(E_F)$ for a PM6:Y6 blend film inferred by ER-EIS. The dashed lines indicate Gaussian fits. The arrow indicates the energetic HOMO–LUMO gap. The vertical lines indicate the energetic positions of the HOMO and LUMO levels of a neat PM6 (yellow) and Y6 (red) film, respectively. c) Table with energetic position E_0 and linewidth σ of DOSs of HOMO and LUMO from PM6, Y6 and PM6:Y6 films. d) Energy scheme of HOMO and LUMO positions for PM6, Y6 and PM6:Y6 film as inferred by ER-EIS measurements.

gap of the blend inferred from the ER-EIS spectrum we arrive at a binding energy of ≈ 150 meV for the CT state. Considering that the estimated Coulomb energy of a pair of point-like charges with intra-pair separation of 1 nm in a medium with a dielectric constant of 3.5 is 410 meV, it is obvious that the spectroscopically determined binding energy of the CT state is significantly reduced. Recalling that the binding energy of a singlet exciton in a neat Y6 (vide supra) is also unusually low we conjecture that both observations have a common origin, namely the delocalization of the electron within an Y6 dimer and the delocalization of the hole in the polymer.

In order to check this conjecture we calculated the Coulombic binding energy of an electron-hole pair with an intra-pair separation of 1 nm embedded in a medium with a dielectric constant of 3.5 as a function of electron-hole separation employing the effective mass model for the hole in the polymer developed earlier.^[40] It involves solving the 1D Schrödinger equation for the hole in the presence of the potential created by an electron that is either localized on a single site or delocalized between two units (1/2 e on

two sites), three units (1/3 e on three sites), or four units (1/4 e on four sites), respectively, with the electron sites being perpendicular to the axis of the chain that carries the hole on the polymeric PM6 donor. Delocalization of the hole is taken into account via its effective mass. We find that for an e–h-pair with charge separation 1 nm, in which the electron is localized on a single site and the hole is delocalized on the polymer with a relative effective mass of 0.1, the binding energy $E_{b,CT}$ is 0.25 eV (Figure 4). Replacing a monomeric acceptor by a J-like dimer with a center of mass separation of 1.5 nm, reduces $E_{b,CT}$ to ≈ 150 meV, which is consistent with the spectroscopically determined CT-state-energy. This simple reasoning demonstrates that dimerization of the acceptor combined with hole-delocalization of the in the polymer lowers the binding energy of a CT state, yet it does not explain why the measured thermal activation energy for photo-dissociation in a PM6:Y6 blend is as low as 6 meV.^[7]

To solve this puzzle, one has to consider that CT dissociation is a kinetically determined process in which recombination of the CT state, quantified by the rate constant k_{rec} , and dissociation,

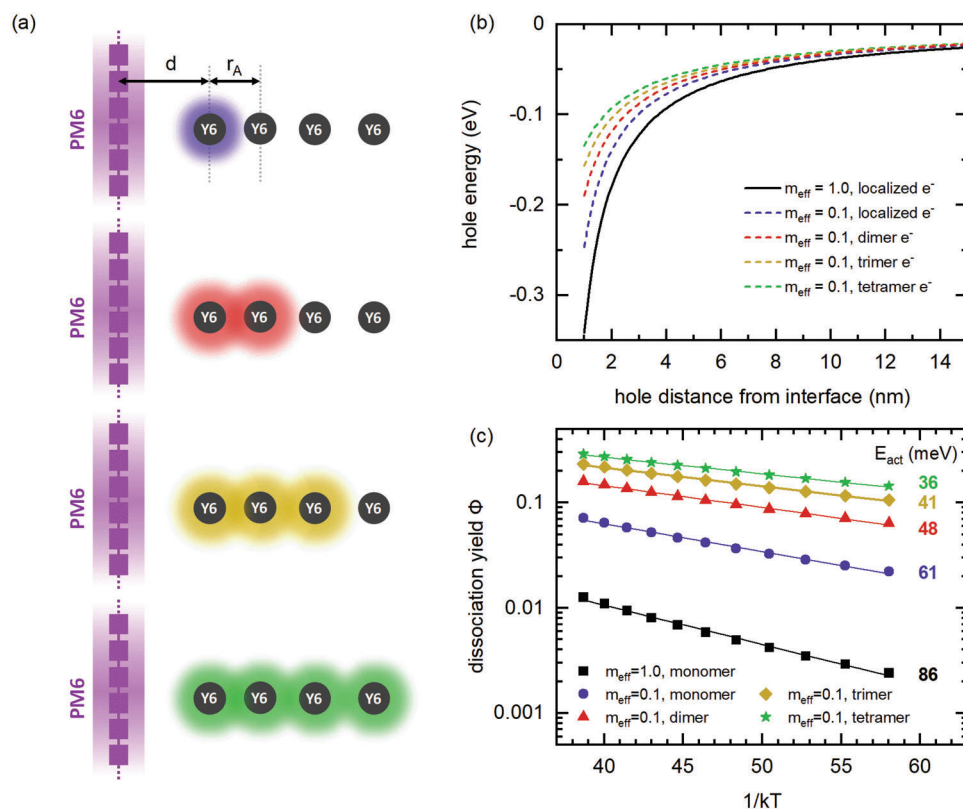


Figure 4. a) Schematic illustrating the geometry between the donor polymer segment (purple squares) and the acceptor molecule (circles) for the case where the electron is extended over one, two, three, and four molecules. Here, r_A is the intra-pair separation and d is the distance between the center-of-mass of the wavefunctions for electron and hole, b) Coulomb potential and c) Dissociation yield, for the hole on the donor polymer segment for the case of a localized hole on the donor and an electron localized on a single acceptor molecule (black), and for the cases of a delocalized hole on the donor ($m_{\text{eff}} = 0.1$) and the electron extended over one, two, three, and four acceptor molecules as indicated in the legend.

quantified by rate constant k_{diss} are competing processes. The k_{diss} is the product of a prefactor rate $k_{\text{diss},0}$ and a Boltzmann factor, $k_{\text{diss}} = k_{\text{diss},0} \exp(-E_{\text{b,CT}}/kT)$ with $E_{\text{b,CT}}$ being the Coulomb energy of the CT state. The dissociation yield is $\phi = k_{\text{diss}}/(k_{\text{diss}} + k_{\text{rec}})$. Suppose that $k_{\text{rec}} \gg k_{\text{diss}}$, for instance, because recombination is controlled by charge carrier hopping among nearest neighbor molecules. In this case the yield is $\phi = (k_{\text{diss},0}/k_{\text{rec}}) \exp(-E_{\text{b,CT}}/kT)$, i.e. the temperature dependence of ϕ is Arrhenius-like and the activation energy is $E_{\text{b,CT}}$. An example is geminate pair recombination of electron-hole pairs tractable in terms of Onsager's 1938 formalism.^[41] In the opposite case, $k_{\text{diss}} \gg k_{\text{rec}}$, the yield approaches unity. Although the individual dissociation event does cost thermal energy, the overall yield is, in this case, independent of temperature because the activated dissociation event is completed before the CT state could decay intrinsically. Obviously, the temperature dependence of photo-dissociation then does not reflect the true binding energy of the CT state and can, indeed, be negligible.

We will substantiate this reasoning in terms of an analytical hopping model.^[49] We will start with the simplest case and consider a 1D random walk of an electron in an array of statistically disordered hopping sites with a standard deviation of 100 meV in the presence of a stationary hole on a polymer chain characterized by a relative effective mass of either 1 or 0.1. When the electron approaches its sibling, it can form a CT state whose life-

time is considered to be 3000 times the pre-factor rate constant (ν_0) for the activated motion of the hole, e.g., $\tau_{\text{CT}} = 30$ ns and $k_{\text{diss},0} = 10^{11} \text{ s}^{-1}$. In the simulations, we assume that the electric field is $5 \times 10^4 \text{ V cm}^{-1}$ and $\epsilon = 3.5$. The result of the simulations is shown in Figure 4c. Intuitively, it is astonishing that even for case of $m_{\text{eff}} = 1$ the activation energy for dissociation is only 86 meV although the Coulomb energy is 350 meV (Figure 4b). This is a signature of the great impact moderate disorder has on the escape process of an e-h pair.^[1,49,50] Note also that the activation energy for CT-dissociation is principally different from the binding energy of the CT state because its escape from the Coulomb potential is not a one step process but rather a multi-step random walk, yet the simulated activation energy for CT dissociation is still finite, contrary with experiment. The reason is that in the simulations of Figure 4, the hole is considered to remain stationary, contrary to the experiment. In earlier, more detailed kMC simulations^[9] the case of bipolar transport had been this limitation has been taken care of. They showed that the inclusion of bipolar transport does increase the dissociation yield considerably. The reason is that when both partners of an e-h pair separated by the phase boundary are both mobile, the probability to meet and form a CT state is greatly reduced and geminate recombination is greatly reduced. In efficient organic solar cells geminate pair recombination is, in fact, negligible.^[1] The activation energy further decreases when the hole is

delocalized along the polymer chain and, in addition, when the electron is shared among the partners of an aggregate. In fact, wavefunction delocalization in Y6 dimers has been reported to facilitate charge separation in blends^[42–44] while the role of vibronic coupling,^[45] hot exciton dissociation,^[46] and entropy^[47] have also been acknowledged to contribute to charge separation in donor–acceptor systems. In an earlier publication, we have shown that although dimensionality and entropic effects increase the overall separation yield, they do not influence the activation energy for charge separation.^[9] Moreover, experiments and simulations have shown that efficient charge separation occurs mainly through cold charge transfer states.^[48,49]

4. Conclusion

Employing energy-resolved impedance spectroscopy, we determined the distribution of hole and electron transporting states in neat films of PM6 and Y6, as well as their blends. It turns out that the HOMO and LUMO spectrum of the blend is basically the superposition of the spectra of the components. No additional features are formed upon blending, only defect-related features in the spectra of neat Y6 film are eliminated. From the analysis of the ER-EIS combined with published photoluminescence spectra of PM6:Y6 blends, we find that the binding energy of the CT state of ≈ 150 meV, i.e., 250 meV lower than the Coulomb binding energy expected for an isolated, localized e–h-pair with 1 nm separation. The reason is that the hole is delocalized on the polymer chain and the electron is shared among two or more molecules because Y6 forms J-like aggregates, yet dissociating a CT state should cost thermal energy, contrary with experiment.

To solve this question, one must consider that the yield of CT state dissociation is determined by the competition between intrinsic recombination of the CT state, associated with rate constant $k_{\text{rec}} = 1/\tau$, τ being the lifetime of the CT state, and its dissociation with rate constant k_{diss} . There are several reasons why in a PM6:Y6 solar cell the condition $k_{\text{diss}} \gg k_{\text{rec}}$ is fulfilled and, therefore, virtually all CT states dissociate under short circuit conditions. The cell is a blend of a well-ordered polymeric donor and an acceptor that tends to form domains in which the elements are electronically J-like coupled dimers. This ensures electronic delocalization in both the donor and the acceptor phase, which reduces the Coulomb attraction of the CT pair. Further advantages are that the charge carrier mobilities are moderately high ($> \approx 10^{-4}$ cm² Vs⁻¹) and the aggregates in Y6 arrange to crystallites that allow for percolation pathways. This ensures that the electron of the CT exciton can quickly diffuse away from its sibling at the phase boundary and has very little chance to recombine geminately with it. The existence of a quadrupole of Y6 may also contribute to preventing geminate recombination.^[7] Overall, the combination of energetic disorder, the existence of percolation pathways, hole delocalization along the PM6 backbone, and electron delocalization enabled by aggregation of Y6 molecules allows for highly efficient barrierless CT state dissociation.

Acknowledgements

The authors acknowledge support through the Bayerisches Staatsministerium für Wissenschaft und Kunst (“Solar Technologies Go Hybrid”),

the German Science Foundation (IRTG 2818 OPTEXC), the Deutsche Forschungsgemeinschaft through the project “MARS” (project number 445281755 (KO3973/8-1)) and the Scientific Grant Agency in Slovakia (VEGA project no. 2/0165/22).

Open access funding enabled and organized by Projekt DEAL.

Conflict of Interest

The authors declare no conflict of interest.

Data Availability Statement

The data that support the findings of this study are available from the corresponding author upon reasonable request.

Keywords

aggregates, exciton dissociation, organic solar cell

Received: March 4, 2023

Revised: April 25, 2023

Published online:

- [1] L. Perdigón-Toro, L. Q. Phuong, F. Eller, G. Freychet, E. Saglamkaya, J. I. Khan, Q. Wei, S. Zeiske, D. Kroh, S. Wedler, A. Köhler, A. Armin, F. Laquai, E. M. Herzig, Y. Zou, S. Shoaee, D. Neher, *Adv. Energy Mater.* **2022**, *12*, 2103422.
- [2] J. Yuan, Y. Zhang, L. Zhou, G. Zhang, H.-L. Yip, T.-K. Lau, X. Lu, C. Zhu, H. Peng, P. A. Johnson, M. Leclerc, Y. Cao, J. Ulanski, Y. Li, Y. Zou, *Joule* **2019**, *3*, 1140.
- [3] F. Liu, L. Zhou, W. Liu, Z. Zhou, Q. Yue, W. Zheng, R. Sun, W. Liu, S. Xu, H. Fan, L. Feng, Y. Yi, W. Zhang, X. Zhu, *Adv. Mater.* **2021**, *33*, 2100830.
- [4] T. Zhang, C. An, P. Bi, Q. Lv, J. Qin, L. Hong, Y. Cui, S. Zhang, J. Hou, *Adv. Energy Mater.* **2021**, *11*, 2101705.
- [5] Q. Guo, Q. Guo, Y. Geng, A. Tang, M. Zhang, M. Du, X. Sun, E. Zhou, *Mater. Chem. Front.* **2021**, *5*, 3257.
- [6] T. P. A. van der Pol, B. T. van Gorkom, W. F. M. van Geel, J. Littmann, M. M. Wienk, R. A. J. Janssen, *Adv. Energy Mater.* **2023**, *13*, 2300003.
- [7] L. Perdigón-Toro, H. Zhang, A. Markina, J. Yuan, S. M. Hosseini, C. M. Wolff, G. Zuo, M. Stolterfoht, Y. Zou, F. Gao, D. Andrienko, S. Shoaee, D. Neher, *Adv. Mater.* **2020**, *32*, 1906763.
- [8] C. Schwarz, H. Bässler, I. Bauer, J.-M. Koenen, E. Preis, U. Scherf, A. Köhler, *Adv. Mater.* **2012**, *24*, 922.
- [9] S. Athanasopoulos, F. Schauer, V. Nádaždy, M. Weiß, F.-J. Kahle, U. Scherf, H. Bässler, A. Köhler, *Adv. Energy Mater.* **2019**, *9*, 1900814.
- [10] J. Yan, E. Rezasoltani, M. Azzouzi, F. Eisner, J. Nelson, *Nat. Commun.* **2021**, *12*, 3642.
- [11] A. Markina, K.-H. Lin, W. Liu, C. Poelking, Y. Firdaus, D. R. Villalva, J. I. Khan, S. H. K. Paleti, G. T. Harrison, J. Gorenflot, W. Zhang, S. De Wolf, I. McCulloch, T. D. Anthopoulos, D. Baran, F. Laquai, D. Andrienko, *Adv. Energy Mater.* **2021**, *11*, 2102363.
- [12] D. Neusser, B. Sun, W. L. Tan, L. Thomsen, T. Schultz, L. Perdigón-Toro, N. Koch, S. Shoaee, C. R. McNeill, D. Neher, S. Ludwigs, *J. Mater. Chem. C* **2022**, *10*, 11565.
- [13] V. Nádaždy, F. Schauer, K. Gmucová, *Appl. Phys. Lett.* **2014**, *105*, 142109.
- [14] F. Schauer, V. Nádaždy, K. Gmucová, T. Váry, *J. Appl. Phys.* **2018**, *124*, 165702.

- [15] H. Bäessler, D. Kroh, F. Schauer, V. Nádaždy, A. Köhler, *Adv. Funct. Mater.* **2021**, *31*, 2007738.
- [16] L. Perdigón-Toro, L. Q. Phuong, S. Zeiske, K. Vandewal, A. Armin, S. Shoaee, D. Neher, *ACS Energy Lett.* **2021**, *6*, 557.
- [17] L. Zhu, J. Zhang, Y. Guo, C. Yang, Y. Yi, Z. Wei, *Angew. Chem.* **2021**, *133*, 15476.
- [18] D. Kroh, F. Eller, K. Schötz, S. Wedler, L. Perdigón-Toro, G. Freychet, Q. Wei, M. Dörr, D. Jones, Y. Zou, E. M. Herzig, D. Neher, A. Köhler, *Adv. Funct. Mater.* **2022**, *32*, 2205711.
- [19] V. I. Arkhipov, P. Heremans, E. V. Emelianova, G. J. Adriaenssens, H. Bäessler, *Appl. Phys. Lett.* **2003**, *82*, 3245.
- [20] N. Geacintov, M. Pope, *J. Chem. Phys.* **1967**, *47*, 1194.
- [21] R. R. Chance, C. L. Braun, *J. Chem. Phys.* **1976**, *64*, 3573.
- [22] S. Barth, H. Bäessler, U. Scherf, K. Müllen, *Chem. Phys. Lett.* **1998**, *288*, 147.
- [23] G. F. Burkhard, E. T. Hoke, M. D. McGehee, *Adv. Mater.* **2010**, *22*, 3293.
- [24] M. N. Polyanskiy, "Refractive index database," can be found under <https://refractiveindex.info> (accessed: February 2023).
- [25] R. Kerremans, C. Kaiser, W. Li, N. Zarrabi, P. Meredith, A. Armin, *Adv. Opt. Mater.* **2020**, *8*, 2000319.
- [26] M. Pope, C. E. Swenberg, *Annu. Rev. Phys. Chem.* **1984**, *35*, 613.
- [27] L. Zhu, M. Zhang, J. Xu, C. Li, J. Yan, G. Zhou, W. Zhong, T. Hao, J. Song, X. Xue, Z. Zhou, R. Zeng, H. Zhu, C.-C. Chen, R. C. I. MacKenzie, Y. Zou, J. Nelson, Y. Zhang, Y. Sun, F. Liu, *Nat. Mater.* **2022**, *21*, 656.
- [28] K. Jiang, Q. Wei, J. Y. L. Lai, Z. Peng, H. K. Kim, J. Yuan, L. Ye, H. Ade, Y. Zou, H. Yan, *Joule* **2019**, *3*, 3020.
- [29] G. Yao, Y. Ge, X. Xiao, L. Zhang, N. Yi, H. Luo, S. Yuan, W. Zhou, *ACS Appl. Energy Mater.* **2022**, *5*, 1193.
- [30] L. Zhu, M. Zhang, G. Zhou, T. Hao, J. Xu, J. Wang, C. Qiu, N. Prine, J. Ali, W. Feng, X. Gu, Z. Ma, Z. Tang, H. Zhu, L. Ying, Y. Zhang, F. Liu, *Adv. Energy Mater.* **2020**, *10*, 1904234.
- [31] Z. Bi, K. Chen, L. Gou, Y. Guo, X. Zhou, H. B. Naveed, J. Wang, Q. Zhu, J. Yuan, C. Zhao, K. Zhou, S. Chandrabose, Z. Tang, Y. Yi, J. M. Hodgkiss, L. Zhang, W. Ma, *J. Mater. Chem. A* **2021**, *9*, 16733.
- [32] Q. Zhao, H. Lai, H. Chen, H. Li, F. He, *J. Mater. Chem. A* **2021**, *9*, 1119.
- [33] J. Xue, H. B. Naveed, H. Zhao, B. Lin, Y. Wang, Q. Zhu, B. Wu, Z. Bi, X. Zhou, C. Zhao, K. Zhou, W. Ma, *J. Mater. Chem. A* **2022**, *10*, 13439.
- [34] Y. Yu, R. Sun, T. Wang, X. Yuan, Y. Wu, Q. Wu, M. Shi, W. Yang, X. Jiao, J. Min, *Adv. Funct. Mater.* **2021**, *31*, 2008767.
- [35] R. Ma, T. Yang, Y. Xiao, T. Liu, G. Zhang, Z. Luo, G. Li, X. Lu, H. Yan, B. Tang, *Energy Environ. Mater.* **2022**, *5*, 977.
- [36] H. Zhao, H. B. Naveed, B. Lin, X. Zhou, J. Yuan, K. Zhou, H. Wu, R. Guo, M. A. Scheel, A. Chumakov, S. V. Roth, Z. Tang, P. Müller-Buschbaum, W. Ma, *Adv. Mater.* **2020**, *32*, 2002302.
- [37] Y. Zhang, Y. Lang, G. Li, *EcoMat* **2023**, *5*, e12281.
- [38] S. Alam, V. Nádaždy, T. Váry, C. Friebe, R. Meitzner, J. Ahner, A. Anand, S. Karuthedath, C. S. P. D. Castro, C. Göhler, S. Dietz, J. Cann, C. Kästner, A. Konkin, W. Beenken, A. M. Anton, C. Ulbricht, A. Sperlich, M. D. Hager, U. Ritter, F. Kremer, O. Brüggemann, U. S. Schubert, D. A. M. Egbe, G. C. Welch, V. Dyakonov, C. Deibel, F. Laquai, H. Hoppe, *J. Mater. Chem. C* **2021**, *9*, 14463.
- [39] L. V. Lukin, *Chem. Phys.* **2021**, *551*, 111327.
- [40] S. Tscheuschner, H. Bäessler, K. Huber, A. Köhler, *J. Phys. Chem. B* **2015**, *119*, 10359.
- [41] L. Onsager, *Phys. Rev.* **1938**, *54*, 554.
- [42] S. Liang, S. Li, Y. Zhang, T. Li, H. Zhou, F. Jin, C. Sheng, G. Ni, J. Yuan, W. Ma, H. Zhao, *Adv. Funct. Mater.* **2021**, *31*, 2102764.
- [43] R. Wang, C. Zhang, Q. Li, Z. Zhang, X. Wang, M. Xiao, *J. Am. Chem. Soc.* **2020**, *142*, 12751.
- [44] G. Zhang, X.-K. Chen, J. Xiao, P. C. Y. Chow, M. Ren, G. Kupgan, X. Jiao, C. C. S. Chan, X. Du, R. Xia, Z. Chen, J. Yuan, Y. Zhang, S. Zhang, Y. Liu, Y. Zou, H. Yan, K. S. Wong, V. Coropceanu, N. Li, C. J. Brabec, J.-L. Bredas, H.-L. Yip, Y. Cao, *Nat. Commun.* **2020**, *11*, 3943.
- [45] S. M. Falke, C. A. Rozzi, D. Brida, M. Maiuri, M. Amato, E. Sommer, A. De Sio, A. Rubio, G. Cerullo, E. Molinari, C. Lienau, *Science* **2014**, *344*, 1001.
- [46] G. Grancini, M. Maiuri, D. Fazzi, A. Petrozza, H.-J. Egelhaaf, D. Brida, G. Cerullo, G. Lanzani, *Nat. Mater.* **2013**, *12*, 29.
- [47] S. N. Hood, I. Kassal, *J. Phys. Chem. Lett.* **2016**, *7*, 4495.
- [48] K. Vandewal, S. Albrecht, E. T. Hoke, K. R. Graham, J. Widmer, J. D. Douglas, M. Schubert, W. R. Mateker, J. T. Bloking, G. F. Burkhard, A. Sellinger, J. M. J. Fréchet, A. Amassian, M. K. Riede, M. D. McGehee, D. Neher, A. Salleo, *Nat. Mater.* **2014**, *13*, 63.
- [49] S. Athanasopoulos, H. Bäessler, A. Köhler, *J. Phys. Chem. Lett.* **2019**, *10*, 7107.
- [50] D. Balzer, T. J. A. M. Smolders, D. Blyth, S. N. Hood, I. Kassal, *Chem. Sci.* **2021**, *12*, 2276.